RECONSTRUCTING THE SPATIAL DISTRIBUTION OF ACOUSTIC CHARACTERISTICS BY TECHNIQUE OF ANGLE HARMONICS

© 2025 D. I. Zotov, O. D. Rumyantseva, A. S. Cherniaev*

Department of Acoustics, Faculty of Physics, Lomonosov Moscow State University, Moscow, Russia

**e-mail: burov@phys.msu.ru*

Received September 06, 2024

Revised September 16, 2024

Accepted September 30, 2024

Abstract. Improved numerical implementation of the two-dimensional functional analytical algorithm is proposed. The algorithm is designed to reconstruct spatial distributions of sound speed and absorption coefficient in a tomography region. The high accuracy of obtained tomograms is illustrated even with large wave sizes and complicated internal structure of object under study.

Keywords: *acoustic tomography, sound velocity and absorption retrieval, functional algorithm, angular harmonics*

DOI: 10.31857/S03676765250118e4

INTRODUCTION

Let us consider a rigorous wave solution of the inverse problem of acoustic scattering. It is required to recover the inhomogeneous spatial distributions of sound velocity $c(\vec{r})$ and amplitude absorption coefficient $\alpha(\vec{r},\omega_j)$ at a given frequency ω_j inside a tomographic object located in the region $\Re$. Outside the region $\Re$ there is a homogeneous non-absorbing background medium; its sound velocity c_0 and wave

number $k_{0j} = \omega_j / c_0$. The transmitters and receivers used to obtain experimental data are outside the region $\Re$ and surround the object under investigation on all sides. The object is probed by a fixed incident acoustic pressure field $u_0(\vec{r})$. Upon reaching the object, this field $u_0(\vec{r})$ is scattered on acoustic inhomogeneities inside $\Re$. This creates a total field $u(\vec{r})$, which is detected by all receivers. The direction of the incident field is then changed, and the corresponding fields $u(\vec{r})$ are again received. The complete data set is obtained by enumerating all possible sensing and receiving directions. This data set is processed, i.e. the inverse problem is solved. As a result, the desired functions $c(\vec{r})$ and $\alpha(\vec{r}, \omega_j)$ are recovered quantitatively. The possibility of obtaining quantitative estimates at each point of $\vec{r}$ space is a fundamental difference between inverse acoustic problems of tomographic type and inverse problems of ultrasound type. This possibility is provided, firstly, by the availability of experimental data at the most different angles and, secondly, by a sufficiently rigorous algorithm for processing such data. Below, for processing purposes, we consider a two-dimensional wave functional-analytic algorithm [1 -5] in the monochromatic version. This algorithm is based on the ideas of solving inverse scattering problems on quantum mechanical potentials [1–3, 6, 7].

The total field $u(\vec{r})$ at each fixed $u_0(\vec{r})$ obeys the Helmholtz equation $\nabla^2 u(\vec{r}) + k_{0j}^2 u(\vec{r}) = v(\vec{r}) u(\vec{r})$, where $v(\vec{r}, \omega_j) = \omega_j^2 \left(\frac{1}{c_0^2} - \frac{1}{c^2(\vec{r})} \right) - i 2\omega_j \frac{\alpha(\vec{r}, \omega_j)}{c(\vec{r})}$ is the scatterer function for time-dependent fields $\sim \exp(-i\omega_j t)$. The function $v(\vec{r}, \omega_j)$ [8] must first be recovered, after which the separate functions $c(\vec{r})$ and $\alpha(\vec{r}, \omega_j)$ [9] can be extracted from it. The input data for the functional algorithm are the complex values of the classical

scattering amplitude $f(\vec{k},\vec{l};\omega_j)$. They are assumed to be known for all valid wave vectors $\vec{k}, \vec{l} \in \mathbb{R}^2$, where $\vec{k}^2 = \vec{l}^2 = k_{0j}^2$. Let the incident field be a classical plane wave

$$u_0(\vec{r},\vec{k};\omega_j) = \exp(i\vec{k}\vec{r}) \tag{1}$$

with wave vector $\vec{k}$, and the field $u(\vec{r},\vec{k};\omega_j)$ is taken in the far field in the direction co-directional to the wave vector $\vec{l}$, i.e., $\vec{r} \uparrow\uparrow \vec{l}$. Then the values $f(\vec{k},\vec{l};\omega_j)$ are proportional to the scattered field $u(\vec{r},\vec{k};\omega_j) - u_0(\vec{r},\vec{k};\omega_j)$. At the same time, the values of $f(\vec{k},\vec{l};\omega_j)$ can be recalculated from the fields taken in the near zone outside the region of the tomographic object [8, 10].

TWO-DIMENSIONAL FUNCTIONAL ALGORITHM AND ANGULAR HARMONIC APPARATUS

The two-dimensional functional algorithm for recovering the scatterer function $v(\vec{r},\omega_j)$ consists of several successive steps, which are given below in terms of angles and angular harmonics [4, 5]. Namely, the angular spectrum $\tilde{g}(q)$ for an arbitrary periodic function $g(\varphi)$ with period 2π is defined by the relations (angular harmonics have integer numbers $q = 0, \pm 1, \pm 2, \ldots$, i.e.,): $q \in \mathbb{Z}$

$$\tilde{g}(q) = \frac{1}{2\pi}\int_0^{2\pi} g(\varphi)\,\exp(-iq\varphi)\,d\varphi, \quad g(\varphi) = \sum_{q=-\infty}^{\infty} \tilde{g}(q)\exp(iq\varphi), \quad q \in \mathbb{Z}. \tag{2}$$

For the two-dimensional vectors $\vec{k}$ and $\vec{l}$ in the polar coordinate system we have:

$$\vec{k} = \{k_{0j},\varphi\}, \quad \vec{l} = \{k_{0j},\varphi'\}; \tag{3}$$

then $f(\vec{k},\vec{l};\omega_j) \equiv f(\varphi,\varphi';\omega_j)$. First, two functions $h^{\pm}(\varphi,\varphi';\omega_j)$ - the so-called generalized scattering amplitude - are found based on the known values of the classical scattering

amplitude $f(\varphi,\varphi';\omega_j)$. For this purpose, for each fixed value of φ , a linear system of equations is solved, which is obtained by enumerating all angles φ' :

$$h^{\pm}(\varphi,\varphi';\omega_j) - \pi i \int_0^{2\pi} h^{\pm}(\varphi,\varphi'';\omega_j)\ \theta\left[\pm\sin(\varphi''-\varphi)\right] f(\varphi'',\varphi';\omega_j)\,d\varphi'' = f(\varphi,\varphi';\omega_j)\ , \quad (4)$$

where $\theta(t) = \{1 \text{ при } t>0; \quad 0 \text{ при } t\le 0\}$ is the Heaviside function. After that, for each fixed point $\vec{r}$ with Cartesian coordinates $\vec{r}=\{x,y\}$ we construct auxiliary functions

$$\begin{aligned} &Q^{\pm}(\vec{r},\varphi,\varphi';\omega_j) \equiv \\ &\equiv h^{\pm}(\varphi,\varphi';\omega_j)\ \exp\left[ik_{0j}\{x(\cos\varphi'-\cos\varphi)+y(\sin\varphi'-\sin\varphi)\}\right]\cdot\theta[\pm\sin(\varphi'-\varphi)]\ . \end{aligned} \quad (5)$$

Their dual angular spectrum is calculated by the Fourier transform in angles:

$$\tilde{\tilde{Q}}^{\pm}(\vec{r},q,q';\omega_j) \equiv \frac{1}{(2\pi)^2}\int_0^{2\pi} d\varphi \int_0^{2\pi} d\varphi'\ Q^{\pm}(\vec{r},\varphi,\varphi';\omega_j)\exp(-iq\varphi)\exp(-iq'\varphi')\ , \quad (6)$$

and for all $q'\in\mathbb{Z}$ the function

$$\tilde{\tilde{B}}(\vec{r},q,q';\omega_j) = \begin{cases} i\pi\tilde{\tilde{Q}}^{-}(\vec{r},q,q';\omega_j) \text{ при } q=0,1,2,3,\ldots; \\ i\pi\tilde{\tilde{Q}}^{+}(\vec{r},q,q';\omega_j) \text{ при } q=-1,-2,\ldots \end{cases} \quad (7)$$

Knowing $\tilde{\tilde{B}}(\vec{r},q,q';\omega_j)$ allows us to find the angular harmonics $\tilde{\mu}^{\text{cl}}(\vec{r},q;\omega_j)$ of a classical field with the "carrier" wave removed: $\mu^{\text{cl}}(\vec{r},\vec{k};\omega_j)\equiv\exp(-i\vec{k}\,\vec{r})\,u(\vec{r},\vec{k};\omega_j)$. These angular harmonics are found at each fixed point $\vec{r}$ from the system of linear equations:

$$\tilde{\mu}^{\text{cl}}(\vec{r},q;\omega_j) + 2\pi\sum_{q'=-\infty}^{\infty}\tilde{\tilde{B}}(\vec{r},q,-q';\omega_j)\,\tilde{\mu}^{\text{cl}}(\vec{r},q';\omega_j) = \delta_{q0}\ , \quad (8)$$

where $\delta_{q0}=\{1 \text{ при } q=0; \quad 0 \text{ при } q\ne 0\}$. Finally, the desired scatterer function is calculated from the relation

$$v(\vec{r},\omega_j) =$$

$$= k_{0j}\left(i\frac{\partial}{\partial x}+\frac{\partial}{\partial y}\right)\left\{\tilde{\mu}^{cl}(\vec{r},q=-1;\omega_j)+2i\pi^2\sum_{q'=-\infty}^{\infty}\tilde{\tilde{Q}}^{-}(\vec{r},q=-1,-q';\omega_j)\,\tilde{\mu}^{cl}(\vec{r},q';\omega_j)\right\}. \qquad (9)$$

The described two-dimensional functional algorithm allows to take into account the processes of multiple wave scattering on inhomogeneities of the medium almost strictly (with accuracy up to the effects associated with backscattering). In this case, all solved systems of equations (4) and (8) remain linear with respect to the unknowns. Nevertheless, the numerical realization of the algorithm [4, 5] is very nontrivial. In the numerical realization it turns out to be convenient to use the apparatus of angular harmonics, which has already been used earlier to record the relations (6)-(9) of this algorithm [4, 5], as well as to correct the experimental data in the case of non-ideal positions of transmitters and receivers [11].

In previous numerical implementations [4, 5], the generalized scattering amplitude $h^{\pm}(\varphi,\varphi';\omega_j)$ was found from the system (4) directly in terms of the angles φ and φ' . The auxiliary functions $Q^{\pm}(\vec{r},\varphi,\varphi';\omega_j)$ were formed, according to (5), also in terms of angles, followed by a double Fourier transform on the angles (6). Subsequent actions (7)-(9) were performed already in terms of angular harmonics [4, 5].

Below it is proposed to solve the system (4) and to consider the relation (5) at once with the help of angular harmonics. Such a technique allows, first, to increase the accuracy of numerical realization when passing from continuous values of angles φ and φ' to discrete numbers of angular harmonics q and q' . Secondly, the relations (4) and (5) contain Heaviside functions

$$\theta^{\pm}(\varphi) \equiv \theta(\pm\sin\varphi)\ , \qquad (10)$$

which change discontinuously from 1 to 0 in the infinitesimal neighborhood of the zero value of its argument. Therefore, the angular discretization step for the functions $\theta^{\pm}(\varphi)$ should be much shallower than for $f(\varphi,\varphi';\omega_j)$ and $h^{\pm}(\varphi,\varphi';\omega_j)$. This is related to the fact that the angular spectrum $\widetilde{\theta}^{\pm}(q) \equiv \frac{1}{2\pi}\int_0^{2\pi} \theta^{\pm}(\varphi)\exp(-iq\varphi)\,d\varphi$ of the functions $\theta^{\pm}(\varphi)$ decays slowly:

$$\widetilde{\theta}^{\pm}(q) = \frac{1}{2}(\mp i)^q \operatorname{sinc}\left(\frac{\pi}{2}q\right) \equiv \left\{ \frac{1}{2} \text{ при } q=0\,; \quad \pm\frac{i}{2\pi q}\left\{(-1)^q - 1\right\} \text{ при } q \neq 0 \right\}, \tag{11}$$

and , $\widetilde{\theta}^{-}(q) = \left\{\widetilde{\theta}^{+}(q)\right\}^{*}\ \forall q$. At the same time, there is a function in ( ) 5

$$E(\vec{r},\varphi,\varphi';\omega_j) \equiv \exp\left[ik_{0j}\{x(\cos\varphi'-\cos\varphi)+y(\sin\varphi'-\sin\varphi)\}\right] \equiv \exp\left\{i(\vec{l}-\vec{k})\vec{r}\right\}, \tag{12}$$

where (3) is taken into account. The function $E(\vec{r},\varphi,\varphi';\omega_j)$ oscillates with changes in φ and φ' the stronger the larger the fixed value of $k_{0j}|\vec{r}|$. As a consequence, the angular spectrum of this function will have the higher significant angular harmonics the larger $k_{0j}|\vec{r}|$. Thus, the introduction of discrete analogs of both functions (10) and (12) requires increased attention in the numerical implementation of the considered functional algorithm.

Thirdly, the consideration of functions in terms of angular harmonics makes it convenient to control the sufficiency of the volume of discretized function values involved at each stage of the restoration procedure. Such control, starting from the volume of initial discretized data $f(\varphi,\varphi';\omega_j)$, is fundamental for ensuring the uniqueness, stability and, ultimately , adequacy of the solution of the considered

inverse problem [8]. This will be briefly mentioned at the stage of numerical simulation.

To transform the integral term of the equations (4), the functions $h^{\pm}(\varphi,\varphi'';\,\omega_j)$ and $f(\varphi'',\varphi';\,\omega_j)$ can be represented according to (2) as

$$h^{\pm}(\varphi,\varphi'';\,\omega_j)=\sum_{q''=-\infty}^{\infty}\widetilde{h}^{\pm}(\varphi,q'';\,\omega_j)\,\exp(iq''\varphi'')\ ,$$

$$f(\varphi'',\varphi';\,\omega_j)=\sum_{q'''=-\infty}^{\infty}\widetilde{f}(q''',\varphi';\,\omega_j)\,\exp(iq'''\varphi'')\ .$$

This brings the equation (4) into the form:

$$h^{\pm}(\varphi,\varphi';\,\omega_j)-\pi i\sum_{q''=-\infty}^{\infty}\sum_{q'''=-\infty}^{\infty}\widetilde{h}^{\pm}(\varphi,q'';\,\omega_j)\,\widetilde{f}(q''',\varphi';\,\omega_j)\times$$
$$\times 2\pi\,\exp\left[i(q''+q''')\varphi\right]\cdot\widetilde{\theta}^{\pm}\left[-(q''+q''')\right]=f(\varphi,\varphi';\,\omega_j)\ .$$

The Fourier transform of this expression over the angle φ' gives:

$$\widetilde{h}^{\pm}(\varphi,q';\,\omega_j)-2i\pi^2\sum_{q''=-\infty}^{\infty}\left\{\sum_{q'''=-\infty}^{\infty}\widetilde{\theta}^{\pm}(-q''-q''')\,\widetilde{\widetilde{f}}(q''',q';\,\omega_j)\,\exp(iq'''\varphi)\right\}\times$$
$$\times\exp(iq''\varphi)\,\widetilde{h}^{\pm}(\varphi,q'';\,\omega_j)=\widetilde{f}(\varphi,q';\,\omega_j);\quad q'\in\mathbb{Z}\ . \tag{13}$$

The system of equations (13) obtained by enumerating $q'\in\mathbb{Z}$, is solved with respect to the single angular harmonics $\widetilde{h}^{\pm}(\varphi,q';\,\omega_j)$ at each fixed angle φ . In the right-hand side (13) stands the single angular spectrum of the classical scattering amplitude

$$\widetilde{f}(\varphi,q';\,\omega_j)=\frac{1}{2\pi}\int_0^{2\pi}f(\varphi,\varphi';\,\omega_j)\,\exp(-iq'\varphi')\,d\varphi'\ ,\quad q'\in\mathbb{Z}\,, \tag{14}$$

and in the left part - the double angular spectrum

$$\widetilde{\widetilde{f}}(q,q';\,\omega_j)=\frac{1}{(2\pi)^2}\int_0^{2\pi}d\varphi\int_0^{2\pi}d\varphi'\,f(\varphi,\varphi';\,\omega_j)\exp(-iq\varphi)\,\exp(-iq'\varphi')\ ,\quad q,q'\in\mathbb{Z}\,. \tag{15}$$

After finding $\widetilde{h}^{\pm}(\varphi,q';\,\omega_j)$, the double angular spectrum is calculated

$$\tilde{\tilde{h}}^{\pm}(q,q';\,\omega_j)=\frac{1}{2\pi}\int_0^{2\pi}\tilde{h}^{\pm}(\varphi,q';\,\omega_j)\exp(-iq\varphi)\,d\varphi\ . \tag{16}$$

On the other hand, it is possible to find at once the dual angular harmonics $\tilde{\tilde{h}}^{\pm}(q,q';\,\omega_j)$ from a system that is obtained by the Fourier transform of the equations (13) on the angle φ followed by substitution of the variables:

$$\begin{gathered}\tilde{\tilde{h}}^{\pm}(q,q';\,\omega_j)-2i\pi^2\sum_{q''=-\infty}^{\infty}\left\{\sum_{q'''=-\infty}^{\infty}\tilde{\tilde{f}}(-q'''+q-q'',\,q';\,\omega_j)\cdot\tilde{\theta}^{\pm}(q'''-q)\right\}\times\\ \times\,\tilde{\tilde{h}}^{\pm}(q''',q'';\,\omega_j)\ =\tilde{\tilde{f}}(q,q';\,\omega_j)\,;\qquad q,q'\in\mathbb{Z}\ .\end{gathered} \tag{17}$$

However, unlike the system (13), which is solved at each fixed φ , the system (17) requires finding $\tilde{\tilde{h}}^{\pm}(q,q';\,\omega_j)$ for all values of (q,q') , i.e., none of the arguments q or q' can be fixed. Thus, the transition from (13) to (17) is not always reasonable, since there may be difficulties due to matrices of huge dimension when solving the system (17) - similar to the situation described in [12].

Instead of performing the sequence of operations (5) and (6), the expression (5) can be transformed immediately in terms of angular harmonics. Taking into account (1), (3) and (12), we have: $E(\vec{r},\varphi,\varphi';\,\omega_j)=\exp(-i\vec{k}\vec{r})\,\exp(i\vec{l}\,\vec{r})\equiv P(\vec{r},\varphi+\pi;\,\omega_j)\,P(\vec{r},\varphi';\,\omega_j)$. Here, for convenience, the notation $u_0(\vec{r},\vec{k};\,\omega_j)\equiv P(\vec{r},\varphi;\,\omega_j)=\exp(i\vec{k}\vec{r})$ is introduced, and then

$$-\vec{k}=\left\{k_{0j},\,\varphi+\pi\right\}\ ,P(\vec{r},\varphi+\pi;\,\omega_j)\equiv\ \exp(-i\vec{k}\vec{r})\ ;\ ,\ .\qquad \vec{l}=\left\{k_{0j},\varphi'\right\}$$

$$P(\vec{r},\varphi';\,\omega_j)\equiv\ \exp(i\vec{l}\,\vec{r})$$

The expression (5) is rewritten as

$$Q^{\pm}(\vec{r},\varphi,\varphi';\,\omega_j) = h^{\pm}(\varphi,\varphi';\,\omega_j)\,\exp\left\{i(\vec{l}-\vec{k})\vec{r}\right\}\cdot\theta^{\pm}\,(\varphi'-\varphi) \equiv$$
$$\equiv h^{\pm}(\varphi,\varphi';\,\omega_j)\;P(\vec{r},\varphi+\pi;\,\omega_j)\;P(\vec{r},\varphi';\,\omega_j)\;\theta^{\pm}\,(\varphi'-\varphi)\,. \qquad (18)$$

Each of the functions $h^{\pm}$ and P in (18) is represented as a sum of angular harmonics:

$$h^{\pm}(\varphi,\varphi';\,\omega_j) = \sum_{q_1=-\infty}^{\infty}\sum_{q_2=-\infty}^{\infty}\widetilde{\widetilde{h}}^{\pm}(q_1,q_2;\,\omega_j)\,\exp(iq_1\varphi)\,\exp(iq_2\varphi')\;,$$

$$P(\vec{r},\varphi+\pi;\,\omega_j) = \sum_{q_3=-\infty}^{\infty}\widetilde{P}(\vec{r},q_3;\,\omega_j)\,\exp\left\{iq_3(\varphi+\pi)\right\}\;,$$

$$P(\vec{r},\varphi';\,\omega_j) = \sum_{q_4=-\infty}^{\infty}\widetilde{P}(\vec{r},q_4;\,\omega_j)\,\exp(iq_4\varphi')\;, \qquad (19)$$

and a double Fourier transform of the expression (18) is performed on the corners φ and φ' , according to (6). This leads (18) to the form:

$$\widetilde{\widetilde{Q}}^{\pm}(\vec{r},q,q';\,\omega_j) = \sum_{q_1=-\infty}^{\infty}\sum_{q_2=-\infty}^{\infty}\left\{\sum_{q_3=-\infty}^{\infty}(-1)^{q-q_1+q_3}\;\widetilde{P}(\vec{r},\,q-q_1+q_3;\,\omega_j)\times\right.$$
$$\left.\times\,\widetilde{P}(\vec{r},\,q'-q_2-q_3;\,\omega_j)\cdot\widetilde{\theta}^{\pm}(q_3)\right\}\widetilde{\widetilde{h}}^{\pm}(q_1,q_2;\,\omega_j)\,. \qquad (20)$$

Since in the polar coordinate system $\vec{r} = \left\{|\vec{r}|,\,\varphi_{\vec{r}}\right\}$, then

$$P(\vec{r},\varphi;\,\omega_j) \equiv \exp(i\vec{k}\vec{r}) = \exp\left\{ik_{0j}|\vec{r}|\cos(\varphi_{\vec{r}}-\varphi)\right\} = \sum_{q=-\infty}^{\infty} i^q\,J_q(k_{0j}|\vec{r}|)\,\exp\left[iq(\varphi-\varphi_{\vec{r}})\right]\,, \qquad (21)$$

where J_q is the Bessel function of q -th order. From the comparison of (19) and (21) it follows that

$$\widetilde{P}(\vec{r},q;\,\omega_j) = i^q\;\exp(-iq\varphi_{\vec{r}})\;J_q(k_{0j}|\vec{r}|)\,. \qquad (22)$$

Substituting (22) into (20) results in the final expression:

$$\widetilde{\widetilde{Q}}^{\pm}(\vec{r},q,q';\omega_j) = (-i)^{q-q'}\exp\{-i\varphi_{\vec{r}}(q+q')\}\times$$
$$\times\sum_{q_1=-\infty}^{\infty}\sum_{q_2=-\infty}^{\infty}(-i)^{q_2-q_1}\exp\{i\varphi_{\vec{r}}(q_1+q_2)\}\ \kappa^{\pm}(q-q_1,q'-q_2,k_{0j}|\vec{r}|)\ \widetilde{\widetilde{h}}^{\pm}(q_1,q_2;\omega_j),$$

(23)

where

$$\kappa^{\pm}(n,n',k_{0j}|\vec{r}|) \equiv \sum_{q_3=-\infty}^{\infty}(-1)^{q_3}\ J_{n+q_3}(k_{0j}|\vec{r}|)\ J_{n'-q_3}(k_{0j}|\vec{r}|)\cdot\widetilde{\theta}^{\pm}(q_3);\quad n,n'\in\mathbb{Z}. \qquad (24)$$

The expression for $\widetilde{\theta}^{\pm}(q)$ is given in (11). It allows you to transform the expression (24) to take into account that $\widetilde{\theta}^{\pm}(q)=0$ at $|q| = 2,4,6,8,\ldots$:

$$\kappa^{\pm}(n,n',k_{0j}|\vec{r}|) = \frac{1}{2}J_n(k_{0j}|\vec{r}|)\ J_{n'}(k_{0j}|\vec{r}|)\pm$$
$$\pm\frac{i}{\pi}\sum_{m=-\infty}^{\infty}\frac{1}{2m+1}J_{n+2m+1}(k_{0j}|\vec{r}|)\ J_{n'-2m-1}(k_{0j}|\vec{r}|);\quad n,n',m\in\mathbb{Z}. \qquad (25)$$

It is directly apparent from (25) that , $\kappa^{-}(n,n',k_{0j}|\vec{r}|) = \left\{\kappa^{+}(n,n',k_{0j}|\vec{r}|)\right\}^{*}\ \forall n,n'\in\mathbb{Z}$

.

Thus, the sequence of actions in restoring the scatterer function using the angular harmonic apparatus has the following schematic form:

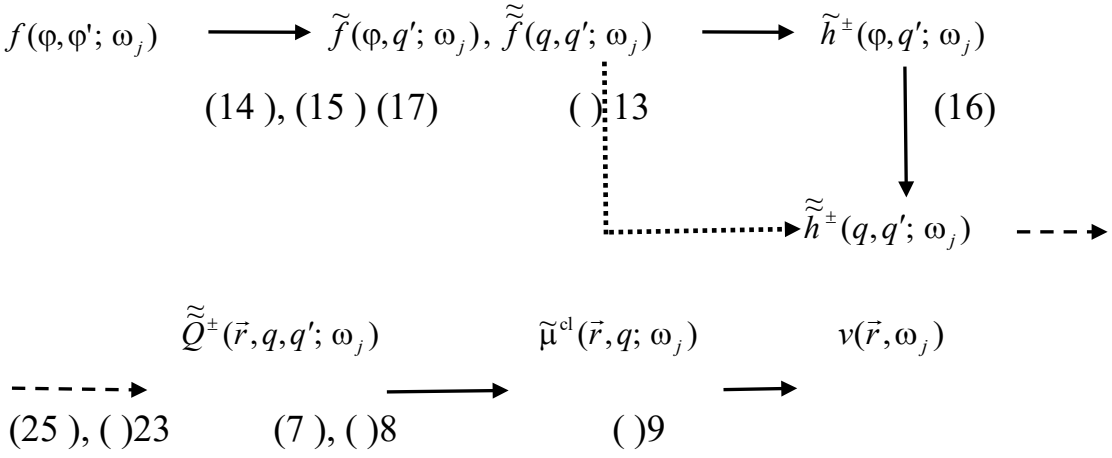

NUMERICAL MODELING

The effectiveness of the proposed new variant of the numerical implementation of the two-dimensional functional algorithm was verified by reconstruction of the model acoustic scatterer. Two MRI images of two-dimensional cross-sections of the breast [13] were taken to specify the scatterer model. One of the images became conventionally interpreted as sound velocity values $c(\vec{r})$ (Fig.1 a), the other image as absorption coefficient values $\alpha(\vec{r},\omega_j)$ (Fig.1 b). In the background non-absorbing medium (water) surrounding the mammary gland, $c_0 = 1500$ m/s was assumed; then the wavelength $\lambda_0 \equiv 2\pi/k_0 = 10^{-3}$ m at the chosen frequency of 1.5 MHz. The sampling step of the images under consideration was set equal to $0.5\lambda_0$. In this case, the entire tomography area was $106\lambda_0$ along each Cartesian axis, and the linear dimension of the breast cross-section proper was $\approx 80\lambda_0$. Quantitative values in the images were set based on the characteristic ranges of $c(\vec{r})$ and $\alpha(\vec{r},\omega_j)$ [14, 15]: assumed to be 1460--1535 m/s for c and 15--34 Np/m, i.e., 1.3--3.0 Db/cm, for α . The values of c and α are largest in skin, and much smaller in subcutaneous adipose tissue.

When the wave travels along the trajectories parallel to the abscissa and ordinate axes, the largest positive additional run-up of the wave phase $\Delta\psi > 0$ is acquired at sites with $c(\vec{r}) > c_0$ [4, 8, 12] along the cross section $y = -\lambda_0$ and is $\Delta\psi \approx 1.25\pi$. The largest (modulo) negative run-up $\Delta\psi < 0$ is acquired at sites with $c(\vec{r}) < c_0$ [4, 8, 12] along the cross section $y = -31\lambda_0$ and is $\Delta\psi \approx -1.27\pi$. The maximum absorption is observed along

the cross section $x = -16.5\ \lambda_0$, while the wave amplitude decreases by a factor of ≈ 8 . Thus, the effects of multiple wave scattering are quite strong.

The 800 quasi-dot transducers were placed uniformly on a circle of radius 0.1536 m around the tomography region. From such data the scattering amplitude was recalculated $f(\varphi,\varphi';\omega_j)$ with the angular sampling step $2\pi/800$. It should be noted that the number of transducers in modern ultrasound tomographs, which are designed primarily for layer-by-layer diagnosis of the breast, can reach one and a half to two thousand [16, 17]. Moreover, additional rotation of the antenna array allows, in principle, to significantly increase the effective volume of experimental information [8].

The double angular spectrum of the scattering amplitude $\tilde{\tilde{f}}(q,q';\omega_j)$ is concentrated near the antidiagonal $q' = -q$. The angular spectrum decreases with high precision to almost zero values at the largest $|q|$ and $|q'|$ (Fig.2 a). This means that the mentioned volume of discretized data $f(\varphi,\varphi';\omega_j)$ encloses almost all the information about the object that can be obtained by off-object field measurements at a given frequency ω_j . This amount of data turns out to be sufficient to reconstruct with good quality the complex spatial structure of the considered scatterer, as well as the values of the sound velocity (Fig.2 b) and absorption coefficient (Fig.2 c). A one-dimensional cross-section of the mammary gland is shown in Fig.2 b and 2c to illustrate the high accuracy of the reconstruction.

CONCLUSION

Thus, the numerical realization of the functional algorithm using the angular harmonic apparatus turned out to be effective. At the same time, in practice, the linear size of the scatterer can be even larger, and the contrast of the sound velocity and absorption coefficient is even stronger than in the considered model. In turn, this further amplifies the effects of multiple wave scattering. Then, in general, a multi-frequency mode is required to ensure stable recovery of the scatterer [5].

FUNDING

The research was supported by the Russian Science Foundation grant No. 24-22-00192, https://rscf.ru/project/24-22-00192/

REFERENCES

1. *Grinevich P.G., Manakov S.V.* // Funct. Anal. Appl. 1986. V. 20. No. 2. P. 94.

2. *Novikov R.G.* // J. Func. Analysis. 1992. V. 103. No. 2. P. 409.

3. *Novikov R.G.* // Phys. Lett. A. 1998. V. 238. No. 2–3. P. 73.

4. *Burov V.A., Rumyantseva O.D.* Inverse wave problems of acoustic tomography. Part 4: Functional-analytical methods for solving multidimensional acoustic inverse scattering problem. M.: LENAND, 2024. 504 c.

4. *Burov V.A., Alekseenko N.V., Rumyantseva O.D.* // Acoust. Phys. 2009. V. 55. No. 6. P. 843.

5. *Faddeev L.D.* // J. Sov. Math. 1976. V. 5. P. 334.

6. *Novikov R.G.* // Int. Math. Res. Papers. 2005. V. 2005. No. 6. P. 287.

8. *Burov V.A., Rumyantseva O.D*. Inverse wave problems of acoustic tomography. Part 2. Inverse problems of acoustic scattering. M.: URSS, 2021. 768 c.

7. *Zotov D.I., Rumyantseva O.D., Shurup A.S.* // Bull. Russ. Acad. Sci. Phys. 2018. V. 82. No. 1. P. 35.

8. *Burov V.A., Shurup A.S., Rumyantseva O.D. et al.* // Bull. Russ. Acad. Sci. Phys. 2012. V. 76. No. 12. P. 1365.

9. *Zotov D.I., Rumyantseva O.D.* // Bull. Russ. Acad. Sci. Phys. 2022. V. 86. No. 1. P. 83.

10. *Zotov D.I., Rumyantseva O.D., Cherniaev A.S.* // Bull. Russ. Acad. Sci. Phys. 2024. V. 88. No. 1. P. 113.

11. https://rentgenogram.ru/dicom-arhiv/molochnye-zhelezy.

12. https://itis.swiss/virtual-population/tissue-properties/database.

13. *Li F., Villa U., Duric N., Anastasio M.A.* // Proc. SPIE. 2023. V. 12470. Art. No. 124700K.

14. *Malik B., Terry R., Wiskin J., Lenox M.* // Med. Phys. 2018. V. 45. No. 7. P. 3063.

15. *Duric N., Sak M., Fan S. et al.* // J. Clin. Med. 2020. V. 9. No. 2. Art. No. 367.

FIGURE CAPTIONS

Fig.1 . Initial model of the acoustic scatterer: spatial distributions of sound velocity (a) and absorption coefficient (b) in a two-dimensional cross-section of the mammary gland.

Fig.2 . Double angular spectrum of the scattering amplitude (a) and the result of the reconstruction (thick dashed line) of the sound velocity (b) and absorption coefficient (c) at $x = 0$ compared to the true values (solid thin line).

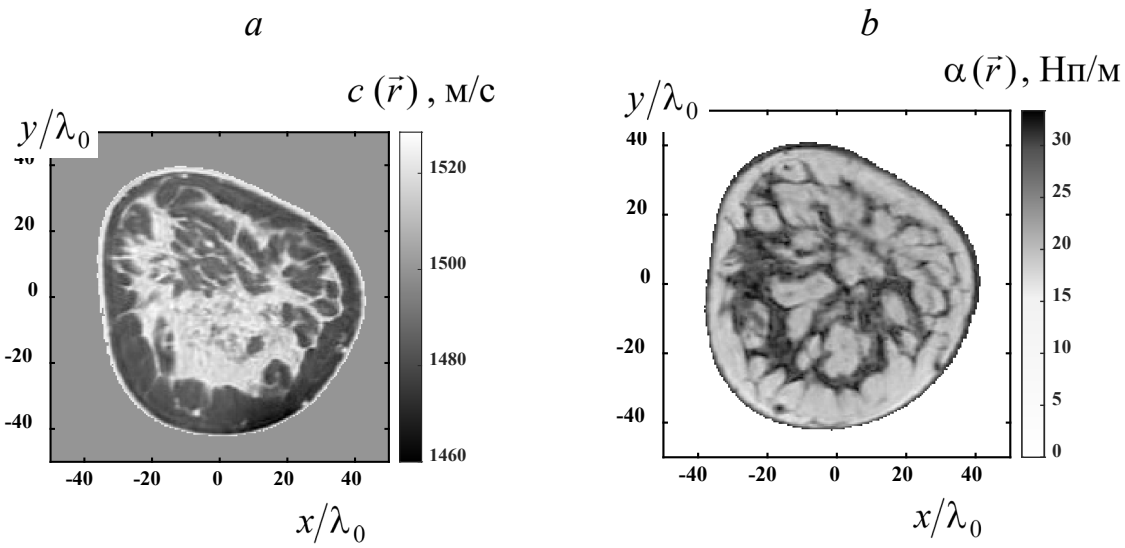

Fig. 1.

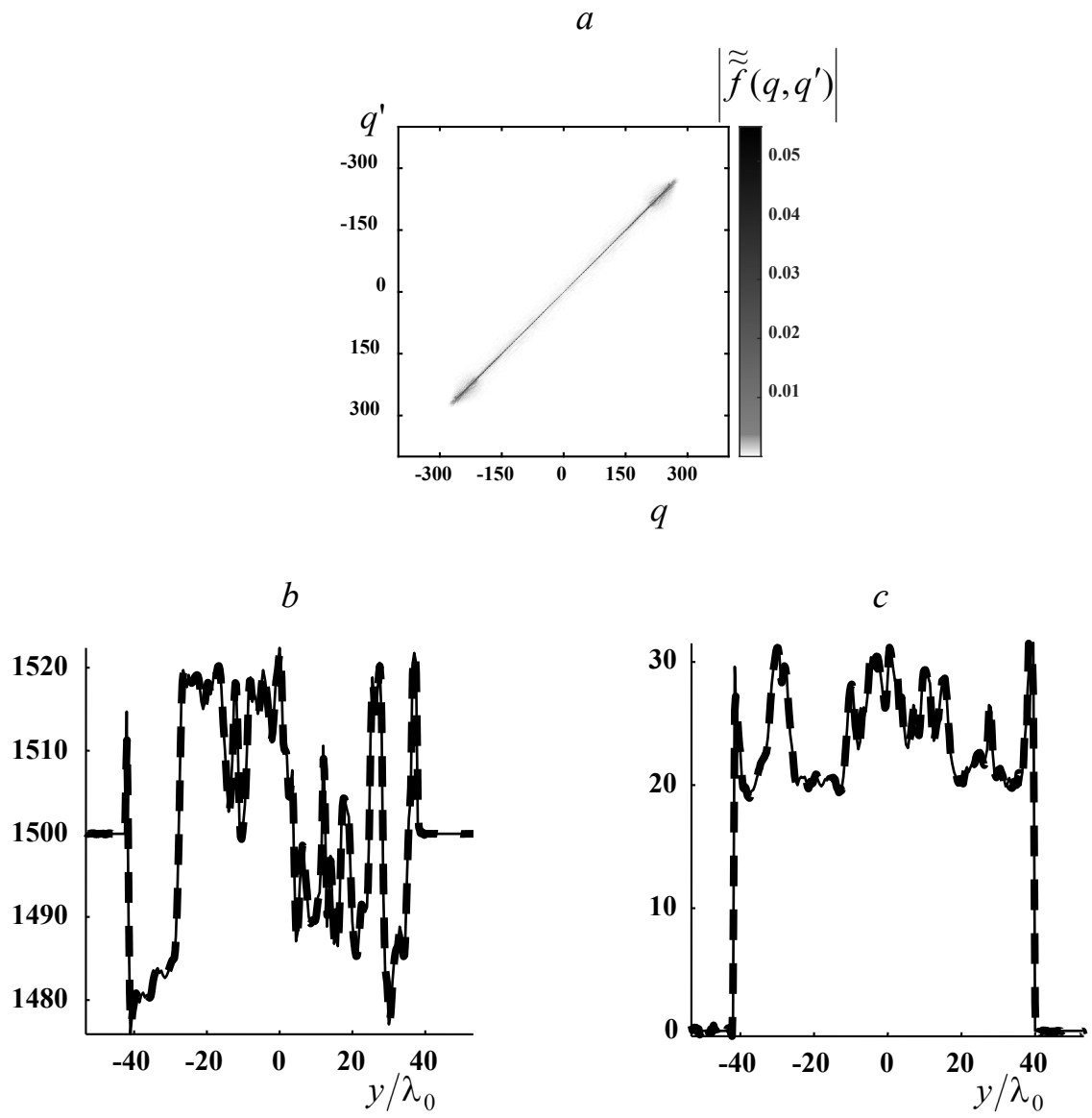
a
$\left|\tilde{\tilde{f}}(q,q')\right|$
q'
-300
-150
0
150
300
0.05
0.04
0.03
0.02
0.01
-300 -150 0 150 300
q
b
1520
1510
1500
1490
1480
-40 -20 0 20 40
y/λ_0
c
30
20
10
0
-40 -20 0 20 40
y/λ_0

Fig. 2.